JACS
JOURNAL OF THE AMERICAN CHEMICAL SOCIETY
Article
Cite This: J. Am. Chem. Soc. XXXX, XXX, XXX−XXX
pubs.acs.org/JACS

# Development of a Series of Practical Fluorescent Chemical Tools To Measure pH Values in Living Samples

Shodai Takahashi,[†,¶] Yu Kagami,[†,¶] Kenjiro Hanaoka,*[,†] Takuya Terai,[‖] Toru Komatsu,[†] Tasuku Ueno,[†] Masanobu Uchiyama,[†,⊥] Ikuko Koyama-Honda,[§] Noboru Mizushima,[§] Tomohiko Taguchi,[†] Hiroyuki Arai,[†] Tetsuo Nagano,[‡] and Yasuteru Urano*[,†,§,#]

[†]Graduate School of Pharmaceutical Sciences, [‡]Drug Discovery Initiative, and [§]Graduate School of Medicine, The University of Tokyo, 7-3-1 Hongo, Bunkyo-ku, Tokyo 113-0033, Japan

[‖]Graduate School of Science and Engineering, Saitama University, 255 Okubo, Sakura-ku, Saitama-shi, Saitama 338-8570, Japan

[⊥]Cluster of Pioneering Research (CPR), Advanced Elements Chemistry Laboratory, RIKEN, 2-1 Hirosawa, Wako, Saitama 351-0198, Japan

[#]CREST (Japan) Agency for Medical Research and Development (AMED), 1-7-1 Otemachi, Chiyoda-ku, Tokyo 100-0004, Japan

Supporting Information

**ABSTRACT:** In biological systems, the pH in intracellular organelles or tissues is strictly regulated, and differences of pH are deeply related to key biological events such as protein degradation, intracellular trafficking, renal failure, and cancer. Ratiometric fluorescence imaging is useful for determination of precise pH values, but existing fluorescence probes have substantial limitations, such as inappropriate p$K_a$ for imaging in the physiological pH range, inadequate photobleaching resistance, and insufficiently long excitation and emission wavelengths. Here we report a versatile scaffold for ratiometric fluorescence pH probes, based on asymmetric rhodamine. To demonstrate its usefulness for biological applications, we employed it to develop two probes. (1) **SiRpH5** has suitable p$K_a$ and water solubility for imaging in acidic intracellular compartments; by using transferrin tagged with **SiRpH5**, we achieved time-lapse imaging of pH in endocytic compartments during protein trafficking for the first time. (2) **Me-pEPPR** is a near-infrared (NIR) probe; by using dextrin tagged with **Me-pEPPR**, we were able to image extracellular pH of renal tubules and tumors in situ. These chemical tools should be useful for studying the influence of intra- and extracellular pH on biological processes, as well as for in vivo imaging.

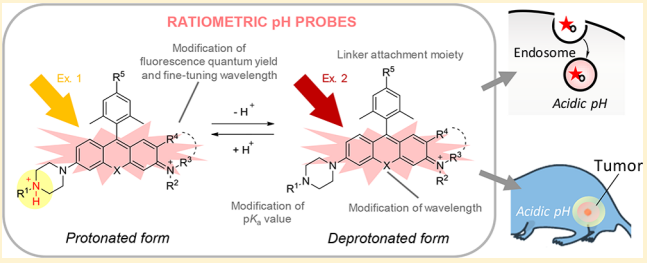


## INTRODUCTION

Control of pH is critical for a variety of biological events, including synthesis and degradation of proteins and trafficking of cell components.[1] To perform these reactions efficiently, intracellular organelles are maintained at specific pH values appropriate for each process.[2,3] Furthermore, not only intracellular pH, but also extracellular pH is important; for example, renal failure causes systemic acidosis,[4] acidic tumors are reported to have higher metastasis ability or proliferation rate,[5] and osteoclasts are activated under acidic conditions.[6]

Fluorescence imaging is a useful technique for pH measurement, offering high spatiotemporal resolution, high sensitivity, and multichannel imaging capacity.[7] In particular, ratiometric fluorescence imaging is an invaluable method for determination of pH, and so far, ratiometric fluorescence probes for pH imaging have been developed.[7−10] However, there has not been reported fluorescence probes for pH imaging in vivo except for two photon excitation fluorescence probe,[11] which is not applicable to image wide range of the tissue. One reason for this is the lack of suitable ratiometric fluorescence probes with both an appropriate p$K_a$ for imaging in the physiological pH range and high photobleaching resistance (essential for long-term imaging).[7] For example, BCECF and SNARF-1, which are a fluorescein derivative and a seminaphthorhodafluor respectively, are conventionally used ratiometric fluorescence probes for pH; however, they possess neutral p$K_a$ values derived from their phenolic group and are also vulnerable to photobleaching.

Recently, we have established synthetic scheme for asymmetric silicon-substituted rhodamines (SiRs).[12] Among them, we discovered a compound that shows an absorption wavelength change of about 80 nm in response to pH change (Figure S1a−c). Rhodamines are often used for fluorescence imaging because of their high resistance to photobleaching, high water solubility, and high fluorescence quantum yields.[13] In addition to these advantages, silicon-substituted rhodamines have longer absorption and emission wavelengths, which enable multicolor imaging with widely used fluorescent proteins such as GFP and YFP.[14−16] So, we considered that silicon-substituted rhodamine could be an excellent scaffold for

Received: January 9, 2018




DOI: 10.1021/jacs.8b00277
J. Am. Chem. Soc. XXXX, XXX, XXX−XXX

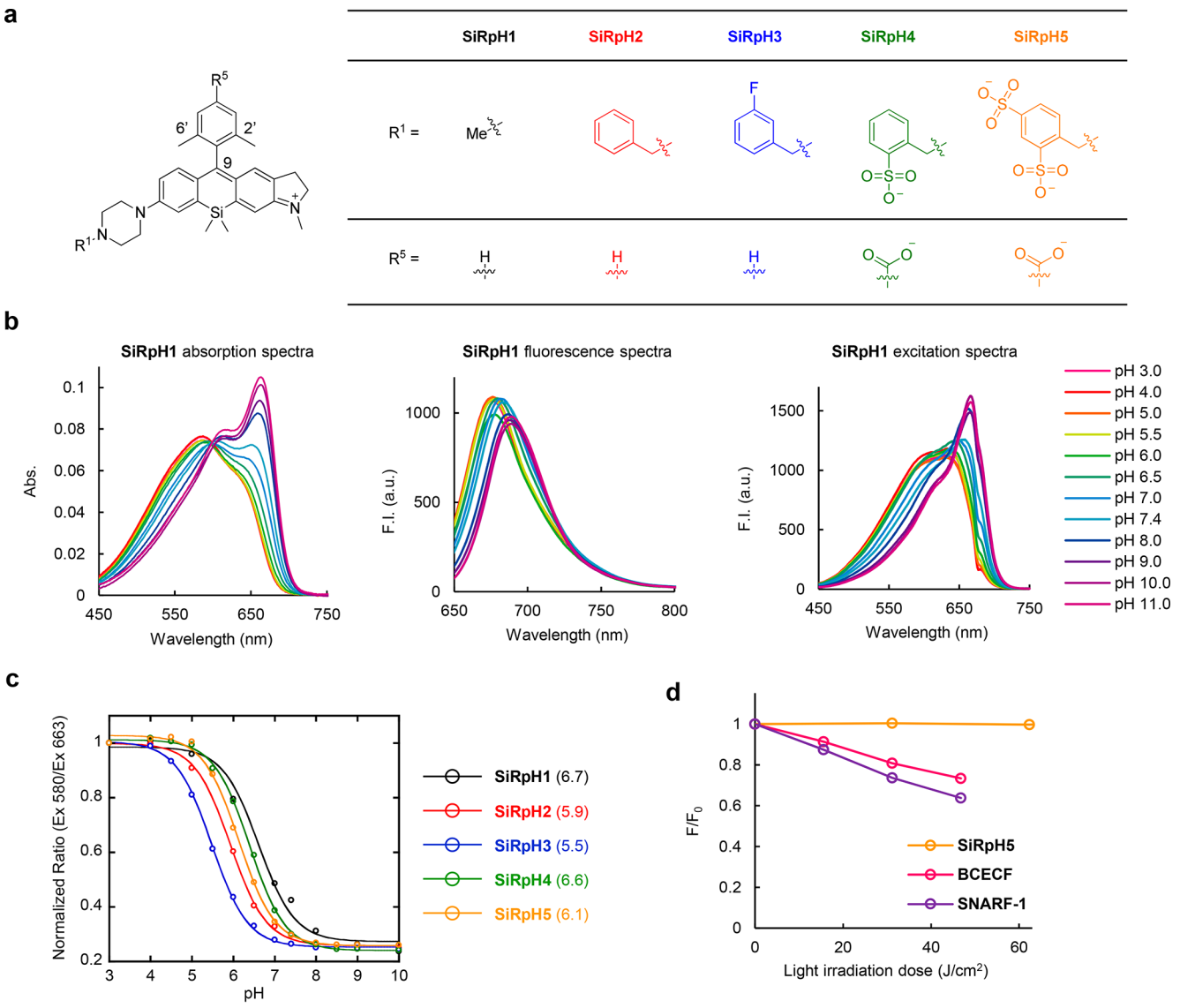


**Figure 1.** Photophysical properties of silicon-substituted rhodamine-based probes for pH. (a) Two methyl groups were introduced at the 2′ and 6′ positions to prevent attack of nucleophiles on the 9 position of the xanthene moiety. In order to optimize the p$K_a$ value, substituent groups were introduced at $R^1$. In order to enable conjugation of probes to other molecules such as macromolecules, a carboxyl group was introduced at $R^5$ for **SiRpH4** and **SiRpH5**. (b) Absorption, fluorescence, and excitation spectra of 2 $\mu$M **SiRpH1** measured in 0.1 M sodium phosphate buffer of various pH values, with 1% DMSO as a cosolvent. Ex = 600 nm (fluorescence spectra); Em = 675 nm (excitation spectra). (c) Ratio of fluorescence intensity at 675 nm excited at 580 nm and that excited at 663 nm is plotted against pH. p$K_a$ values are given in parentheses beside the graph. (d) Fluorescence intensity changes of fluorescent dyes upon light irradiation at pH 7.4. Ex/Em = 610 nm/690 nm (**SiRpH5**), 475 nm/529 nm (BCECF), or 514 nm/627 nm (SNARF).

developing fluorescence probes for ratiometric pH measurements, because modification of the p$K_a$ value and the absorption and emission wavelengths, as well as introduction of functional groups, can be easily performed. Here we report the development of two fluorescence probes based on this scaffold (**SiRpH5** and **Me-pEPPR**), one for imaging of intracellular organelle pH, and the other for imaging of extracellular pH. We confirmed the practical value of these probes by using transferrin tagged with **SiRpH5** for time-lapse imaging of pH in endocytic compartments involved in protein recycling, and by using dextrin tagged with **Me-pEPPR** to image extracellular pH of renal tubules and tumors in situ.

## RESULTS AND DISCUSSION

**Development of a Fluorescence Probe for Ratiometric pH Imaging, SiRpH5.** An asymmetric silicon-substituted rhodamine **8**, which bears a piperazine ring on its xanthene moiety, was discovered to show an absorption shift of about 80 nm to shorter wavelength in acidic aqueous solutions (Figure S1a–c). This spectral shift is comparable to that of conventionally used ratiometric fluorescence probes such as BCECF and SNARF-1.[7] However, it showed a gradual absorption increase at pH 7.0, probably due to dissociation of hydroxide ion from the 9 position of the xanthene ring (Figure S1d,e). To overcome this instability, methyl groups were introduced at both the 2′ position and the 6′ position of the benzene ring in the design of **SiRpH1** (Figure 1a). As we expected, **SiRpH1**


DOI: 10.1021/jacs.8b00277
J. Am. Chem. Soc. XXXX, XXX, XXX−XXX

retained the same pH-responsive change of absorption wavelength as compound **8**, but did not show the time-dependent gradual absorption increase (Figure 1b). Furthermore, both the protonated and deprotonated forms of **SiRpH1** showed high fluorescence intensity. This photophysical property is important for accurate ratiometric imaging, and is in contrast to the case of BCECF, a conventional ratiometric pH probe, which lacks this feature. A plot of the fluorescence intensity ratio of **SiRpH1** at 675 nm excited at 580 nm and at 663 nm showed that the ratio is pH-dependent, with p$K_a$ = 6.7 (Figure 1c). This result confirmed that the asymmetric silicon-substituted rhodamine scaffold with a piperazine ring on the xanthene moiety is a promising scaffold for ratiometric fluorescent pH probes.

In order to image intracellular acidic organelles, the p$K_a$ should be adjusted to be around 5−6.[2,3] Since the fluorescence ratio change of **SiRpH1** is induced by protonation of the amino group on the piperazine ring, we expected that the p$K_a$ of **SiRpH1** could be modified by introducing various substituent groups onto the N atom of the piperazine ring. We tried a benzyl group (**SiRpH2**), a 3-fluorobenzyl group (**SiRpH3**), a 2-sulfobenzyl group (**SiRpH4**), and a 2,4-disulfobenzyl group (**SiRpH5**) (Figure 1a). We previously found that introduction of a benzyl group in place of a methyl group lowers the p$K_a$ of an amino group by about 1.0 unit.[17] Indeed, introduction of the benzyl group lowered the p$K_a$ of **SiRpH2** to 5.9 (**SiRpH1**: 6.7) (Figure 1c, Figure S2a). Introduction of the more electron-withdrawing 3-fluorobenzyl group (**SiRpH3**) resulted in a more acidic p$K_a$ of 5.5 (Figure 1c, Figure S2b). Though the 2-sulfobenzyl group is a strong electron-withdrawing group, the p$K_a$ of **SiRpH4** (6.6) was unexpectedly higher than that of **SiRpH2** (5.9) (Figure 1c, Figure S2c). On the other hand, the p$K_a$ of **SiRpH5** having a 2,4-disulfobenzyl group was 6.1, which should be suitable for imaging acidic intracellular compartments (Figure 1c, Figure S2d). Furthermore, **SiRpH5** showed higher photostability than the widely used ratiometric pH probes BCECF and SNARF-1 (Figure 1d). In addition, the excitation and emission wavelengths of BCECF are shorter than those of **SiRpH5**,[18] and the p$K_a$ values of BCECF and SNARF-1 are 7.0 and 7.5.[18,19] Thus, BCECF and SNARF-1 do not have favorable properties for multicolor imaging with GFP or YFP or for imaging intracellular organelle pH. In contrast, our newly developed ratiometric fluorescence probes have appropriate p$K_a$ values for imaging intracellular acidic organelles, high resistance to photobleaching, and long excitation and emission wavelengths.

**Fluorescence Imaging of pH in Intracellular Compartments.** In order to image luminal pH in intracellular organelles, pH probes were linked to macromolecules that accumulate in specific intracellular compartments. First, we focused on dextran, which is a high-molecular weight polysaccharide composed of glucose as a monomer. Though dextran is basically cell-impermeable, it can be transferred into cells by endocytosis, and is transported from early endosomes to late endosomes, and finally to lysosomes.[20] Among the probes synthesized above, **SiRpH3** and **SiRpH5**, which have sufficiently acidic p$K_a$ values, were used for labeling dextran. Probes bearing succinimidyl ester were conjugated to amino groups of 10 kDa aminodextran to yield **SiRpH3-Dex** and **SiRpH5-Dex** (Figures S3a, S4a). In the case of **SiRpH5-Dex**, a polyethylene glycol (PEG) linker was used. The degree of labeling (DOL) was 1.8 for **SiRpH3-Dex** and 2.6 for **SiRph5-Dex**. **SiRpH3-Dex** and **SiRpH5-Dex** retained the same pH responses as those of **SiRpH3** and **SiRpH5**, respectively (Figures S3b−d, S4b−d), and thus, they work as pH probes even when conjugated to dextran.

In order to investigate whether these dextran conjugates can image lysosomal pH values selectively, **SiRpH3-Dex** or **SiRpH5-Dex** was incubated with cells and fluorescence microscopic imaging was performed. We found that **SiRpH5-Dex** stained lysosomes specifically (showing good colocalization with lysosome marker, Vamp7[21]), while **SiRpH3-Dex** stained not only lysosomes, but also mitochondria (Figure 2a,

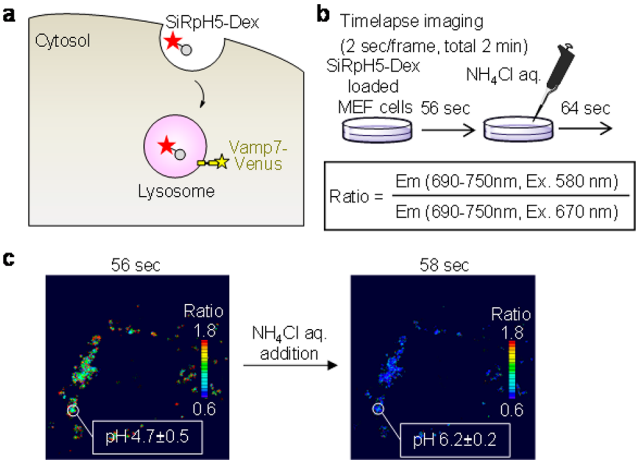


**Figure 2.** Fluorescence imaging of pH in intracellular organelles using **SiRpH5-Dex**. (a) Schematic illustration of endocytic delivery of **SiRpH5-Dex** to lysosomes. (b) Protocol of lysosomal pH imaging. (c) Fluorescence ratio images of the MEF cells before and after addition of $NH_4Cl$ aq.

Figure S5). This nonspecific staining by **SiRpH3-Dex** might be due to the hydrophobicity of **SiRpH3**, i.e., some **SiRpH3** were noncovalently attached to dextran. These results indicated that **SiRpH5** is suitable for specific imaging of lysosomes. Then, we investigated whether **SiRpH5-Dex** can be applied to visualize the change of lysosomal pH upon addition of $NH_4Cl$ or not, which is reported to neutralize lysosomal pH (Figure 2b).[22] Fluorescence ratio images were constructed by dividing the fluorescence intensity at 690−750 nm excited at 580 nm by that excited at 670 nm, and showed a clear increase of pH in lysosomes just after the addition of $NH_4Cl$ (at 56 s), suggesting that neutralization of lysosomal pH by $NH_4Cl$ occurs within seconds (Figure 2c, Supplementary Movie S1). Conversion of the ratio values to pH by means of a calibration curve (Figure S6) indicated that the lysosomal pH was 4.7 before addition of $NH_4Cl$ and 6.2 afterward (Figure 2c), in accordance with reported values.[22] Thought the error bars in the calibration curve are large, it is not because of the lack of brightness of the fluorescence probe (fluorescence quantum yield is comparable to that of conventional fluorophores), and pH values were determined with errors of 0.2−0.5 unit.

Next, we sought to image endosomal pH changes during intracellular trafficking of transferrin (Tfn). Two $Fe^{3+}$ ions bind to Tfn to form holo-Tfn,[23] which binds to Tfn receptors (TfnR) on the plasma membrane, and is internalized by endocytosis into early endosomes (EE), where $Fe^{3+}$ is dissociated from Tfn by the acidic environment. Apo-Tfn/TfnR is then transported to recycling endosomes (RE), and finally exported back to the plasma membrane (Figure 3a).


DOI: 10.1021/jacs.8b00277
J. Am. Chem. Soc. XXXX, XXX, XXX−XXX

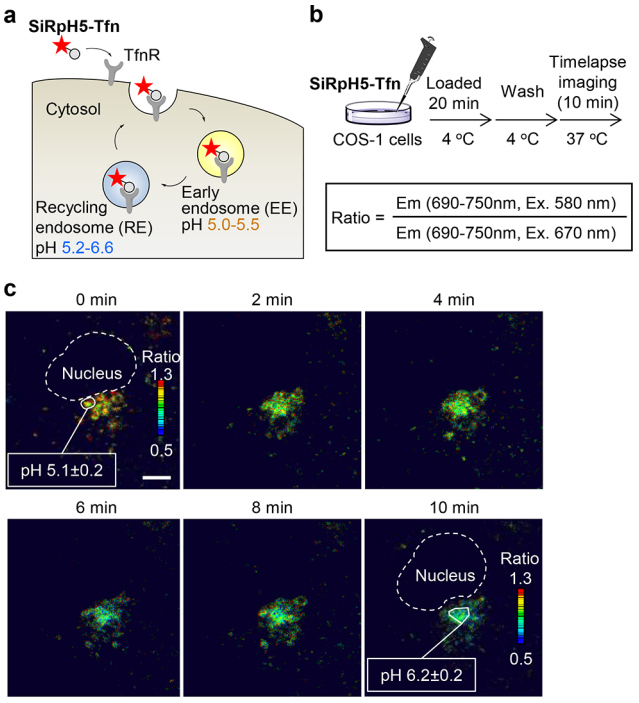


**Figure 3.** Fluorescence imaging of pH in intracellular organelles using **SiRpH5-Tfn**. (a) Schematic illustration of endocytosis of **SiRpH5-Tfn** mediated by transferrin receptor (TfnR). pH values indicated in the figures are cited from the literature.[1,23,24] (b) Protocol of endosomal pH imaging. (c) Time-lapse fluorescence ratio images of the COS-1 cells incubated at 37 °C. Scale bar: 10 $\mu$m.

Although it is known that RE is more basic than EE, time-lapse imaging of endosomal pH during the trafficking of Tfn has not been achieved because of the lack of pH probes with appropriate p$K_a$ and resistance to photobleaching. First, we conjugated **SiRpH5** to holo-Tfn to yield **SiRpH5-Tfn** (DOL was 7.3), and **SiRpH5-Tfn** was confirmed to have almost the same pH response as **SiRpH5** (Figure S7). COS-1 cells were incubated with **SiRpH5-Tfn** for 20 min at 4 °C (endocytosis is blocked at this temperature), and washed. The temperature was then raised to 37 °C, and the time-lapse fluorescence imaging was performed (Figure 3b). This protocol results in synchronized endocytic trafficking of Tfn. Just after the start of incubation at 37 °C, fluorescence of **SiRpH5-Tfn** was colocalized with EE marker GFP-3×FYVE[25−27] (Figure S8a), while after 10 min, it was colocalized with RE marker EGFP-Rab11[24,28] (Figure S8b). This result suggests that **SiRpH5-Tfn** was transported from early endosomes to recycling endosomes similarly to Tfn. Ratiometric fluorescence images showed that endosomal pH was gradually basified (Figure 3c, Supplementary Movie S2). By converting the ratio values of fluorescence intensities to pH values based on the calibration curve (Figure S9), endosomal pH was measured to be 5.1 and 6.2 at 0 and 10 min after incubation at 37 °C, respectively (Figure 3c). Thus, we have succeeded for the first time in time-lapse imaging of the luminal pH of endosomes involved in recycling.

**Development of a NIR Fluorescence Probe for Ratiometric pH Imaging, Me-pEPPR.** For in vivo fluorescence imaging, the NIR wavelength range of 650−900 nm, commonly referred to as the biological optical window,[29] is useful because it affords high tissue penetration compared to visible light (light in the visible region is efficiently absorbed by hemoglobin[29]) and autofluorescence of biomolecules is quite low in this region.[30] But, although several NIR fluorescence probes for ratiometric fluorescence imaging have been developed, they have inappropriate properties for in vivo imaging of pH, i.e., low p$K_a$,[31] low fluorescence quantum yield,[17] or insufficiently long excitation wavelength.[9] Recently, it has been reported that phosphorus-substituted xanthene fluorophores have longer absorption and fluorescence wavelengths than silicon-substituted xanthene fluorophores.[32,33] Although **SiRpH5** has NIR excitation and emission wavelengths in the deprotonated form, its excitation wavelength in the protonated form is not long enough for NIR fluorescence imaging (Figure S2). Therefore, we designed and synthesized a series of phosphorus-substituted asymmetric rhodamines, which we expected would show NIR excitation and emission wavelengths not only in the deprotonated form, but also in the protonated form.

Both of the initially synthesized compounds showed absorption and fluorescence wavelengths in the NIR region (Figures 4a, S10, S11), and **pipediEt-PPhR** (**pEPPR**) showed a higher fluorescence quantum yield than **pipeindo-PPhR** (Figures S10a, S11a). Therefore, we decided to utilize **pEPPR** as a scaffold for NIR fluorescence pH probes. Substitution of silicon to phosphorus at the xanthene 10 position did not affect the pH response of the absorption spectra, and we confirmed that **pEPPR** can be used as a ratiometric fluorescence pH probe (Figure S11c). We also chose 650 and 705 nm as excitation wavelengths for measuring the ratio values of **pEPPR**, because these are within the NIR wavelength range. From the plot of fluorescence ratio against pH, the p$K_a$ of **pEPPR** was calculated to be 7.9, which is not suitable for imaging of neutral to weakly acidic cellular environments in organs and tumors (Figure 4c). The fitting curve of pEPPR was also not completely matched with the pH plots probably because of its water-solubility. Therefore, the p$K_a$ of **pEPPR** was modified by introducing alkyl groups (methyl, ethyl, and *i*-propyl) (Figure 4a,b, Figure S12). The methyl group lowered the p$K_a$ of **pEPPR** from 7.9 to 6.8, which is appropriate for the imaging of neutral to weakly acidic pH (Figure 4c). Thus, **Me-pEPPR** was selected for ratiometric pH imaging experiments.

**Fluorescence Imaging of Organ pH in Vivo.** While intracellular pH is normally neutral (~7.4), except for specific organelles such as lysosomes and endosomes, extracellular pH can easily be changed by various biological events, such as rapid cell proliferation (e.g., cancer cells), and ion resorption in the kidney.[4,5] Therefore, imaging of extracellular pH is important for monitoring biological events in vivo, and for this purpose pH probes should be cell-impermeable. However, when small fluorescent molecules are injected into animals, almost all of them accumulate primarily in liver or kidney and are rapidly excreted, making it difficult to image other organs and tissues.[34] So, we decided to conjugate **Me-pEPPR** with dextran. Owing to its large molecular weight, dextran is cell-impermeable, and it is used for vascular imaging.[35,36] It is well retained inside the body, and its fluorophore conjugate accumulates in tumors as a result of the enhanced permeability and retention (EPR) effect.[37,38] Therefore, we expected that conjugation of **Me-pEPPR** to dextran would afford a probe with cell-impermeability, high retention, and tumor accumulation capability. We also expected that the conjugation with dextran improves the water-solubility of the probe. For our purpose, amino groups of 40 kDa dextran were labeled with **Me-pEPPR** bearing succinimidyl ester to afford dextran-**Me-pEPPR** conjugate,


DOI: 10.1021/jacs.8b00277
J. Am. Chem. Soc. XXXX, XXX, XXX−XXX

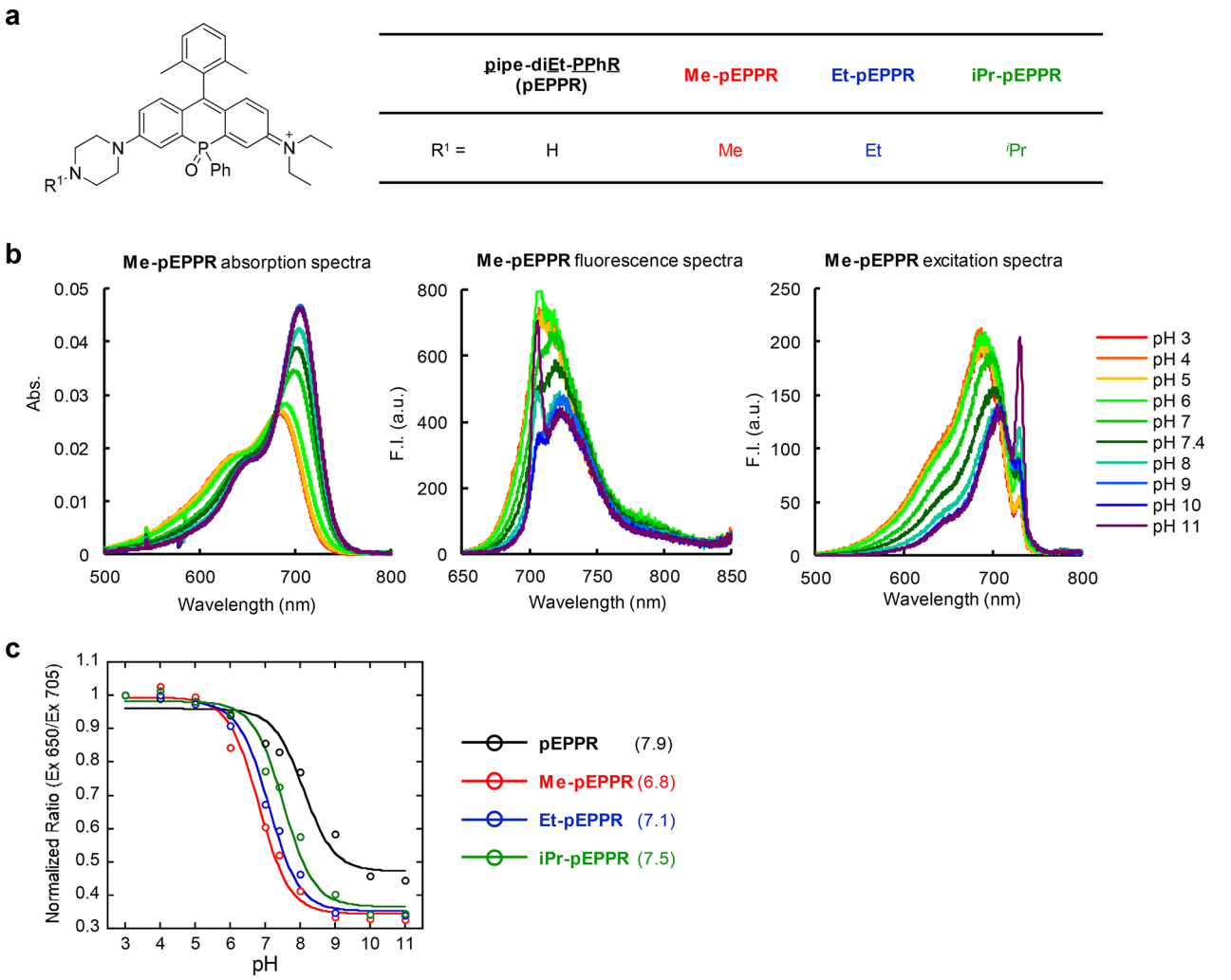


**Figure 4.** Photophysical properties of phosphorus-substituted rhodamine-based probes for pH. (a) In order to optimize p$K_a$, various alkyl groups were introduced at $R^1$. (b) Absorption, fluorescence, and excitation spectra of 1 $\mu$M **Me-pEPPR** measured in 0.1 M sodium phosphate buffer at various pH values, with 0.1% DMSO as a cosolvent. Ex = 705 nm (fluorescence spectra); Em = 730 nm (excitation spectra). (c) Ratio of fluorescence intensity at 730 nm excited at 650 nm and that excited at 705 nm is plotted against pH. p$K_a$ values are given in parentheses beside the graph.

**Dex-Me-pEPPR**. **Dex-Me-pEPPR**s with various degrees of labeling (DOL) were prepared, and their photophysical properties and cell permeability were investigated. Conjugation of **Me-pEPPR** to dextran hardly affected the p$K_a$ value or fluorescence quantum yield of the probe, though some fluorescence quenching was observed when the DOL reached 5.7 (Figure S13). Fluorescence microscopy confirmed that **Dex-Me-pEPPR** with any DOL was cell-impermeable, though **Me-pEPPR** itself was cell-permeable (Figue 5). Thus, it was expected that **Dex-Me-pEPPR** could be used to measure extracellular pH selectively.

As proof of concept, we first attempted to visualize renal tubular pH; this is important, as it can provide insight into renal function.[39] In order to identify the part of the kidney to which **Dex-Me-pEPPR** is distributed, **Dex-Me-pEPPR** was intravenously (i.v.) injected into mice. After 1 h the kidneys were removed, and sections were imaged by fluorescence microscopy. NIR fluorescence was observed from the renal cortex, especially from tubules (Figure S14), which is the same pattern as reported previously.[40] Thus, the probe can be used for pH imaging at renal tubules. It is reported that renal tubular pH is around 6.3−7.0, but is neutralized by carbonic anhydrase

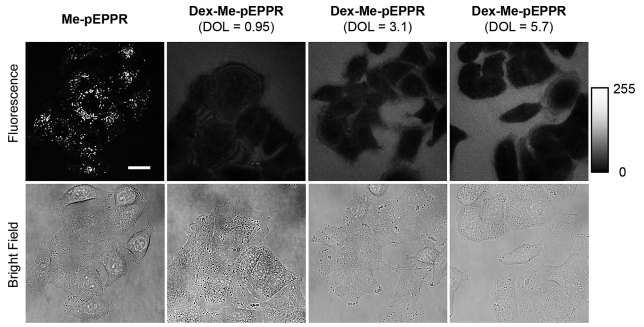


**Figure 5.** Investigation of cell-permeability of **Me-pEPPR** and **Dex-Me-pEPPR**. A549 cells were incubated with 1 $\mu$M **Me-pEPPR** or 5 $\mu$M **Dex-Me-pEPPR** for 30 min at 37 °C and imaged with a confocal fluorescence microscope. Degree of labeling (DOL) of **Me-pEPPR** conjugated to dextran is given above each image. Scale bar: 20 $\mu$m.

inhibitors such as acetazolamide.[41] Therefore, after administration of acetazolamide or saline as a control to mice for a week, the animals were injected with **Dex-Me-pEPPR**, followed by fluorescence ratio imaging 1 h later (Figure 6a).


DOI: 10.1021/jacs.8b00277
J. Am. Chem. Soc. XXXX, XXX, XXX−XXX

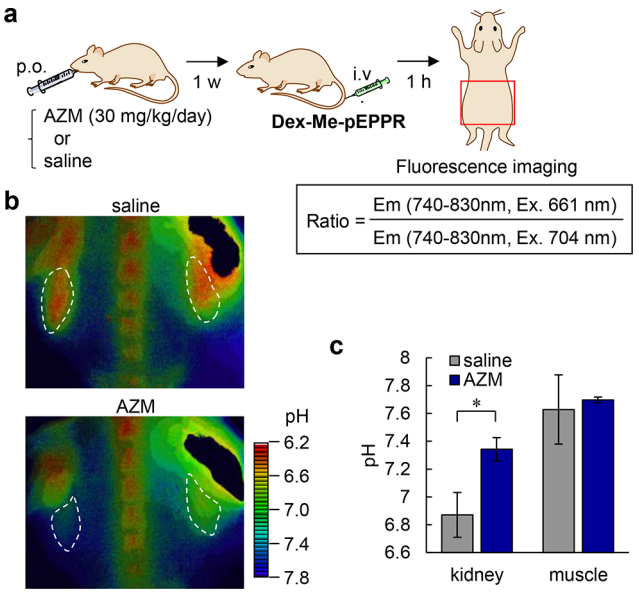


**Figure 6.** In vivo fluorescence imaging of pH at renal tubules using **Dex-Me-pEPPR**. (a) Protocol of renal tubular pH imaging. Saline was administered as a control. The area surrounded by the red square was imaged in b. AZM: acetazolamide. (b) Fluorescence ratio images of mice treated with saline or AZM. Kidneys are indicated with white dotted lines. (c) pH values at kidney and muscle measured by fluorescence imaging. Error bars represent standard errors ($n$ = 3). *$p$ < 0.05.

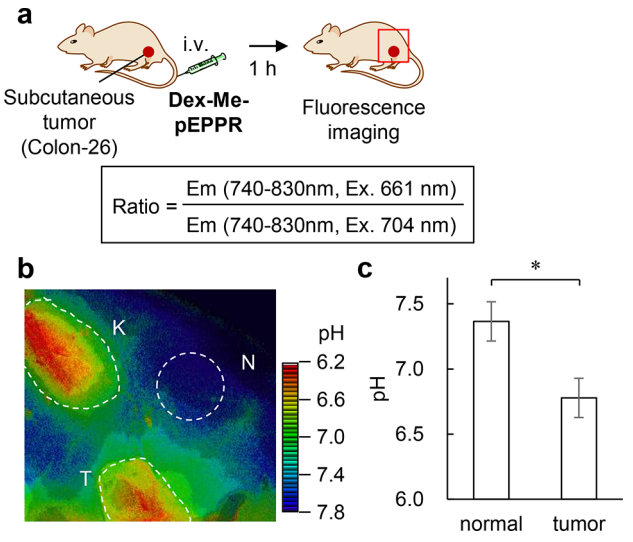


**Figure 7.** In vivo fluorescence imaging of pH at tumors using **Dex-Me-pEPPR**. (a) Protocol of tumoral pH imaging. The area surrounded by the red square was imaged in b. (b) Fluorescence ratio images of mice with subcutaneous tumors. White dotted lines and characters in the figure indicate organ or tissues, respectively. K: kidney, N: normal tissue, T: tumor. (c) pH values at normal tissue and tumor measured by fluorescence imaging. Error bars represent standard errors ($n$ = 11). *$p$ < 0.05.

Fluorescence ratio was converted to pH according to a calibration curve measured in 0.1 M sodium phosphate buffer of various pH values (Figure S15). The results indicated that the renal tubular pH of control mice was 6.9, while that of acetazolamide-treated mice was 7.4 (Figure 6b,c). Thus, **Dex-Me-pEPPR** could visualize pH in the kidney in vivo after i.v. injection.

Finally, we examined pH imaging of tumors with **Dex-Me-pEPPR**. Tumor cells show upregulated glycolysis, which causes intracellular acidification due to overproduction of metabolic acids such as lactate and $CO_2$.[42] In order to survive in this acidic environment, cells overexpress various transporters or enzymes and excrete excess intracellular acids.[43] In consequence, most tumors have an acidic extracellular pH, which may be as low as 6.5–7.0.[5,44] Current techniques for in vivo imaging of tumor pH are based mainly on magnetic resonance imaging (MRI),[45−47] but this requires expensive equipment as well as a long measurement time owing to the low detection sensitivity of MRI contrast agents.[29] A fluorescence-based method should enable relatively high-throughput imaging of tumor pH in vivo. Here, fluorescence ratio imaging was performed 1 h after i.v. injection of **Dex-Me-pEPPR** into mice bearing a subcutaneous tumor (Figure 7a).

Although large fluorescence intensity change was hardly detectable, significant change of fluorescence ratio can be detected at tumor (Figure S16). The tumor pH was measured to be 6.8, corresponding to weak acidification of tumors, while the pH of normal tissue (muscle) was measured to be 7.4 (Figure 7b,c). These pH values measured by ratiometric fluorescence imaging showed good agreement with those measured using a pH electrode (Figure S17). Thus, NIR fluorescence imaging of tumor extracellular pH was successfully achieved for the first time.

## CONCLUSIONS

We have found that asymmetric rhodamines bearing a piperazine ring show a large, pH-dependent blue shift of the absorption spectra upon protonation of the piperazine ring. Time-dependent density functional theory (TDDFT) calculations reproduced well the spectral changes, and the NIR absorption bands observed for **8** and **pEPPR** can be assigned to the HOMO → LUMO transitions (Figure S18). Figure S19 shows the frontier orbitals of these compounds. The HOMO orbitals of the deprotonated forms spread widely from the xanthene ring to the piperazine ring, and the HOMO energy levels are significantly destabilized by the strong antibonding interaction between the two rings, compared to those of the protonated forms. The HOMO−LUMO gaps in the deprotonated forms are increased mainly because the connecting C−N bond lengths in the protonated forms are longer than those in the deprotonated forms, which effectively stabilizes the HOMO energies due to the weaker antibonding interaction, while stabilization of the LUMOs is modest. In addition, the compounds were highly fluorescent in both protonated and deprotonated forms. On the basis of these findings, we were able to fine-tune the probe properties (i.e., p$K_a$, water solubility, and fluorescence quantum yield) in order to obtain the desired ratiometric fluorescence pH probes (**SiRpH5** and **Me-pEPPR**).

**SiRpH5** is a fluorophore whose excitation and emission wavelengths lie in the far-red to NIR region. This provides a new color window for multicolor pH imaging, and indeed, pH imaging with GFP and Venus was achieved in this report. In addition, **SiRpH5** has a higher resistance to photobleaching compared to conventional ratiometric probes, suggesting that **SiRpH5** would be a suitable probe for long-term tracking of intracellular organelle pH. Conjugation of **SiRpH5** to macromolecules was an effective strategy for specific imaging of intracellular organelles, and **SiRpH5** could be delivered to the targeted intracellular organelles by choosing an appropriate


DOI: 10.1021/jacs.8b00277
J. Am. Chem. Soc. XXXX, XXX, XXX−XXX

macromolecule for conjugation. By using **SiRpH5** conjugated with Tfn, endosomal pH change during trafficking of Tfn was imaged for the first time. Moreover, conjugation of the NIR probe to dextran enabled imaging of extracellular pH in vivo. Thus, i.v. injection of **Dex-Me-pEPPR** enabled NIR fluorescence imaging of kidney and tumor pH for the first time. It should be possible to image the pH of other organs, such as gastrointestinal tract, similarly by conjugating the probe to a suitable macromolecule to control the biodistribution.

Thus, the asymmetric rhodamine scaffold is useful for developing functional ratiometric fluorescence probes. In particular, the absorption and emission wavelengths can be modified by changing the 10-position atom of the xanthene moiety and the alkyl group on amino group of the xanthene moiety, while the p$K_a$ value can be modified by changing the substituent group on the piperazine ring. Further, an appropriate targeting moiety can be easily introduced because conjugation does not affect the properties of the probes. We believe ratiometric fluorescence probes based on this novel scaffold will contribute to studies of various biological phenomena associated with pH change, both in organelles of living cells and in organs in situ.

## EXPERIMENTAL SECTION

**Materials and General Information.** Reagents and solvents were of the best grade available, supplied by Tokyo Chemical Industries, Wako Pure Chemical, Aldrich Chemical Co., Dojindo, Kanto Chemical Co., Watanabe Chemical Industries, Matrix Scientific, Thermo Fisher Scientific Inc. and Invitrogen, and were used without further purification. NMR spectra were recorded on a JEOL JNM-LA300 instrument at 300 MHz for $^1$H NMR and at 75 MHz for $^{13}$C NMR, or a JEOL JNM-LA400 instrument at 400 MHz for $^1$H NMR and at 100 MHz for $^{13}$C NMR. All chemical shifts ($\delta$) reported in ppm are relative to internal standard tetramethylsilane ($\delta$ = 0.0 ppm), or relative to the signals of residual solvent $CDCl_3$ (7.26 ppm for $^1$H, 77.16 ppm for $^{13}$C), $CD_3OD$ (3.31 ppm for $^1$H, 49.00 ppm for $^{13}$C), or $CD_3CN$ (1.94 ppm for $^1$H, 1.32 ppm for $^{13}$C), and coupling constants are given in Hz. Mass spectra (MS) were measured with a JEOL JMS-T100LC AccuToF (ESI). HPLC analyses were performed on an Inertsil ODS-3 (4.6 × 250 mm) column (GL Sciences Inc.) using an HPLC system composed of a pump (PU-980, JASCO) and a detector (MD-2015, JASCO). Preparative HPLC was performed on an Inertsil ODS-3 (10.0 × 250 mm) column (GL Sciences Inc.) using an HPLC system composed of a pump (PU-2080, JASCO) and a detector (MD-2015 or FP-2025, JASCO).

**UV−Vis Absorption and Fluorescence Spectroscopy.** UV−visible spectra were obtained on a Shimadzu UV-1650. Fluorescence spectroscopic studies were performed on a Hitachi F4500. The slit width was 5 nm for both excitation and emission. The photomultiplier voltage was 700 V. Absolute quantum yields were measured with a Hamamatsu Photonics Quantaurus QY. Relative fluorescence quantum yields were obtained by comparing the area under the emission spectra of the test samples with standard samples. They were calculated according to the following equation.

$$\Phi_x/\Phi_{st} = [A_{st}/A_x][n_x^2/n_{st}^2][D_x/D_{st}]$$

where st: standard; $x$: sample; $A$: absorbance at the excitation wavelength; $n$: refractive index; $D$: area under the fluorescence spectra on an energy scale.

**Photobleaching Test.** Fluorescence spectra of 1 $\mu$M BCECF, SNARF-1 and **SiRpH5** were measured in 0.1 mM sodium phosphate buffer (pH 7.4) containing 0.1% DMSO as a cosolvent after light irradiation (26 mW, 450−510 nm (BCECF), 26 mW, 515−569 nm (SNARF-1), or 26 mW, 615−695 nm (**SiRpH5**)) using a fiber optic illuminator MAX-301 (Asahi Spectra) equipped with a 150 W xenon lamp (Bunkoukeiki).

**Labeling of Dextran with SiRpH3-SE.** Solutions of 10 kDa aminodextran (Invitrogen) (1.42 mg, 142 nmol) in 284 $\mu$L of 100 mM borate buffer (pH 8.0) and 9 equiv of **SiRpH3-SE** in 57 $\mu$L of DMSO were mixed and stirred at room temperature for 1.5 h. Reaction mixtures were purified on size exclusion PD-10 columns (GE Healthcare) using water as the mobile phase, and the eluate was lyophilized to yield **SiRpH3-Dextran**.

**Labeling of Dextran with SiRpH5-PEG$_6$-SE.** Solutions of 10 kDa aminodextran (1.30 mg, 130 nmol) in 460 $\mu$L of 100 mM $NaHCO_3$ aq. (pH 8.4) and 3.8 equiv of **SiRpH5-PEG$_6$-SE** in 160 $\mu$L of DMSO were mixed and stirred at room temperature for 2 h. Reaction mixtures were purified on size exclusion PD-10 columns using PBS as the mobile phase, and desalted with PD-10 column using water as the mobile phase. The eluate was lyophilized to yield **SiRpH5-Dex**.

**Preparation of Cells.** HeLa cells and COS-1 cells were purchased from American Type Culture Collection (ATCC). A cDNA encoding mouse Vamp7 was obtained as described,[21] and was inserted into pMRXIP (provided by S. Yamaoka, Tokyo Medical and Dental University)[48] together with Venus provided by A. Miyawaki (RIKEN). MEFs stably expressing Venus-Vamp7 were generated using retrovirus infection as previously described.[49] Lung carcinoma cell line, A549 cells were purchased from RIKEN Bioresource Center cell bank (Tsukuba, Japan). Murine colon carcinoma cell line, Colon-26 cells were a gift from Dr. Yoshihiro Hayakawa (University of Toyama, Institute of Natural Medicine). Cells were cultured in Dulbecco's modified Eagle's medium (DMEM) (Invitrogen Corp., Carlsbad, CA) supplemented with 10% fetal bovine serum (Invitrogen), and 1% penicillin streptomycin (Invitrogen). Cells were maintained at 37 °C under an atmosphere of 5% $CO_2$ in air.

**Lysosomal pH Imaging in MEF Cells with SiRpH5-Dex.** 1.6 × 10$^4$ MEF cells stably expressing Vamp7-Venus were seeded on 8-chamber plates (NUNCTM) and cultured for 1 day before imaging. Cells were incubated in 200 $\mu$L of DMEM (10% FBS) containing 200 $\mu$g/mL **SiRpH5-Dex** for 2 h at 37 °C, then washed three times with DMEM, further incubated in DMEM for 3 h at 37 °C, and then imaged using a Leica Application Suite Advanced Fluorescence (LAS-AF) instrument with a TCS SP5 and 63 × oil immersion objective lens. The light source was a white-light laser SuperK (Leica). The excitation and emission wavelengths were 510 nm/530−560 nm for Vamp7-Venus and 580 nm, 670 nm/690−750 nm for **SiRpH5-Dex**.

**Labeling of Holo-transferrin with SiRpH5-PEG$_6$-SE.** Solutions of 80 kDa human holo-transferrin (9.04 mg, 113 nmol) in 1 mL of 100 mM borate buffer (pH 8.0) and 8 equiv of **SiRpH5-PEG$_6$-SE** in 1 mL of 100 mM borate buffer (pH 8.0) containing 20% DMSO were mixed and stirred at room temperature for 1 h. Reaction mixtures were purified by size exclusion PD-10 columns using PBS as the mobile phase, desalted on a PD-10 column using water as the mobile phase, and lyophilized to yield **SiRpH5-Tfn**.

**Endosomal pH Imaging in COS-1 Cells with SiRpH5-Tfn.** 5.0 × 10$^4$ COS-1 cells were seeded on 35 mm poly-L-lysine-coated glass-bottomed dishes (Matsunami Glass Ind., Ltd.), transfected with GFP-3×FYVE or EGFP-Rab11 by using Lipofectamine 2000 (Invitrogen) and cultured for 1 day before imaging. Cells were incubated in 1 mL of HBSS containing 25 $\mu$g/mL **SiRpH5-Tfn** for 20 min at 4 °C, then washed twice with ice-cold HBSS and imaged at 37 °C using a Leica Application Suite Advanced Fluorescence (LAS-AF) instrument with a TCS SP5 and 63× oil immersion objective lens. The light source was a white-light laser SuperK (Leica). The excitation and emission wavelengths were 488 nm/500−530 nm for GFP-3×FYVE, and EGFP-Rab11, and 580 nm, 660 nm/680−750 nm for **SiRpH5-Tfn**.

**Labeling of Dextran with Me-pEPPR.** Solutions of 40 kDa aminodextran (Invitrogen) (2.50 mg, 62.5 nmol) in 250 $\mu$L of 100 mM $NaHCO_3$ aq. (pH 8.4) and 2, 6, or 10 equiv of **Me-pEPPR-SE** in 150 $\mu$L of 100 mM $NaHCO_3$ aq. (pH 8.4) and 100 $\mu$L of DMSO were mixed and stirred at room temperature for 2 h. Reaction mixtures were purified on size exclusion PD-10 columns using PBS as the mobile phase, desalted with PD-10 column using water as the mobile phase, and then lyophilized to yield **Dex-Me-pEPPR**.

**Evaluation of Cell Permeability of Me-pEPPR and Dex-Me-pEPPR.** 1.0 × 10$^5$ A549 cells were seeded on 35 mm poly-L-lysine-


DOI: 10.1021/jacs.8b00277
J. Am. Chem. Soc. XXXX, XXX, XXX−XXX

coated glass-bottomed dishes (Matsunami Glass Ind., Ltd.) and cultured for 1 day before imaging. Cells were washed once with 1 mL of PBS, incubated in probes in DMEM supplemented with 10% fetal bovine serum (Invitrogen), 1% penicillin streptomycin (Invitrogen) containing the probes at 37 °C for 30 min followed by fluorescence imaging with a Leica Application Suite Advanced Fluorescence (LAS-AF) with a TCS SP5 and a 63× oil immersion objective lens. The light source was a white-light laser SuperK (Leica). The excitation and emission wavelengths were 670 nm/700−780 nm.

**In Vivo Imaging of Renal Tubular pH.** All procedures were approved by the Animal Care and Use Committee of the University of Tokyo. Jcl:ICR mice (female, 6-week-old) were purchased from CLEA Japan, Inc. Acetazolamide (30 mg/kg/day) in saline or saline as a control was orally administered for 7 days before imaging. **Dex-Me-pEPPR** (DOL = 1.4) (100 $\mu$M in 140 $\mu$L of saline) was injected intravenously 1 h before imaging. Mice were anesthetized with isoflurane using a small animal anesthetizer MK-A110 (Muromachi Kikai Co., Ltd., Tokyo, Japan), and skin on their back was excised. Then, fluorescence images were captured with a Maestro In Vivo Imaging System (PerkinElmer, Inc., MA, USA) equipped with an excitation filter of 661 nm (641−681 nm) or 704 nm (684−729 nm) and an emission long path filter of 745 nm. Fluorescence ratio was converted to pH value using the standard curve (Figure S15).

**In Vivo Imaging of Tumoral pH.** All procedures were approved by the Animal Care and Use Committee of the University of Tokyo. BALB/cAJcl-nu-nu mice (male, 5−6-week-old) were purchased from CLEA Japan, Inc. $1.0 \times 10^5$ Colon-26 cells were injected on their left flank 1−2 weeks before imaging. **Dex-Me-pEPPR** (DOL = 1.4) (100 $\mu$M in 140 $\mu$L of saline) was injected intravenously 1 h before imaging. Mice were anesthetized with isoflurane using a small animal anesthetizer MK-A110 (Muromachi Kikai Co., Ltd., Tokyo, Japan), and skin near the tumor was excised. Fluorescence images were captured with a Maestro In Vivo Imaging System (PerkinElmer, Inc., MA, USA) equipped with an excitation filter of 661 nm (641−681 nm) or 704 nm (684−729 nm), and an emission long path filter of 745 nm. Fluorescence ratio was converted to pH value using the standard curve (Figure S15).

## ■ ASSOCIATED CONTENT

### Supporting Information

The Supporting Information is available free of charge on the ACS Publications website at DOI: 10.1021/jacs.8b00277.

Experimental procedures, synthesis description, and supporting figures (PDF)

Movie S1 (AVI)

Movie S2 (AVI)

## ■ AUTHOR INFORMATION


### Corresponding Authors

*khanaoka@mol.f.u-tokyo.ac.jp

*uranokun@mol.f.u-tokyo.ac.jp

### ORCID

Kenjiro Hanaoka: 0000-0003-0797-4038

Takuya Terai: 0000-0002-3425-3589

Toru Komatsu: 0000-0002-9268-6964

Masanobu Uchiyama: 0000-0001-6385-5944

Tomohiko Taguchi: 0000-0003-0464-6370

Yasuteru Urano: 0000-0002-1220-6327

### Author Contributions

¶S.T. and Y.K. contributed equally.


### Notes

The authors declare no competing financial interest.

## ■ ACKNOWLEDGMENTS

This work was supported in part by grants by JSPS KAKENHI Grant Numbers 16H00823 and 16H05099 to K.H., 16H06574 to T.U. and KAKENHI (S) (No. 17H06173) (to M.U.) and SENTAN, JST to K.H., who was also supported by a grant JSPS Core-to-Core program, A. Advanced Research Networks, and Mochida Memorial Foundation for Medical and Pharmaceutical Research.

## ■ REFERENCES


(1) Casey, J. R.; Grinstein, S.; Orlowski, J. *Nat. Rev. Mol. Cell Biol.* **2010**, *11*, 50−61.

(2) Teter, K.; Chandy, G.; Quiñones, B.; Pereyra, K.; Machen, T.; Moore, H.-P. H. *J. Biol. Chem.* **1998**, *273*, 19625−19633.

(3) Yamashiro, D. J.; Tycko, B.; Fluss, S. R.; Maxfield, F. R. *Cell* **1984**, *37*, 789−800.

(4) Soriano, J. R. *J. Am. Soc. Nephrol.* **2002**, *13*, 2160−2170.

(5) Neri, D.; Supuran, C. T. *Nat. Rev. Drug Discovery* **2011**, *10*, 767−777.

(6) Rodan, G. A.; Martin, T. J. *Science* **2000**, *289*, 1508−1514.

(7) Han, J.; Burgess, K. *Chem. Rev.* **2010**, *110*, 2709−2728.

(8) Yin, J.; Hu, Y.; Yoon, J. *Chem. Soc. Rev.* **2015**, *44*, 4619−4644.

(9) Li, Y.; Wang, Y.; Yang, S.; Zhao, Y.; Yuan, L.; Zheng, J.; Yang, R. *Anal. Chem.* **2015**, *87*, 2495−2503.

(10) Liu, X.; Su, Y.; Tian, H.; Yang, L.; Zhang, H.; Song, X.; Foley, J. W. *Anal. Chem.* **2017**, *89*, 7038−7045.

(11) Park, H. J.; Lim, C. S.; Kim, E. S.; Han, J. H.; Lee, T. H.; Chun, H. J.; Cho, B. R. *Angew. Chem., Int. Ed.* **2012**, *51*, 2673−2676.

(12) Nagano, T.; Hanaoka, K.; Egawa, T.; Kushida, Y.; Numasawa, K.; Myochin, T.; Piao, W. Asymmetrical Si Rhodamine and Rhodol Synthesis. WO2014106957A1: 2015.

(13) Haugland, R. P., Ed.; *The Handbook, A Guide to Fluorescent Probes and Labeling Technologies*, 10th ed.; Molecuar Probes, Inc.; Eugene, OR, 2005.

(14) Koide, Y.; Urano, Y.; Hanaoka, K.; Piao, W.; Kusakabe, M.; Saito, N.; Terai, T.; Okabe, T.; Nagano, T. *J. Am. Chem. Soc.* **2012**, *134*, 5029−5031.

(15) Egawa, T.; Hanaoka, K.; Koide, Y.; Ujita, S.; Takahashi, N.; Ikegaya, Y.; Matsuki, N.; Terai, T.; Ueno, T.; Komatsu, T.; Nagano, T. *J. Am. Chem. Soc.* **2011**, *133*, 14157−14159.

(16) Kushida, Y.; Nagano, T.; Hanaoka, K. *Analyst* **2015**, *140*, 685−695.

(17) Myochin, T.; Kiyose, K.; Hanaoka, K.; Kojima, H.; Terai, T.; Nagano, T. *J. Am. Chem. Soc.* **2011**, *133*, 3401−3409.

(18) Rink, T. I.; Tsien, R. Y.; Pozzan, T. *J. Cell Biol.* **1982**, *95*, 189−196.

(19) Buckler, K. J.; Vaughan-Jones, R. D. *Pfluegers Arch.* **1990**, *417*, 234−239.

(20) Ohkuma, S.; Poole, B. *Proc. Natl. Acad. Sci. U. S. A.* **1978**, *75*, 3327−3331.

(21) Itakura, E.; Kishi-Itakura, C.; Mizushima, N. *Cell* **2012**, *151*, 1256−1269.

(22) Poole, B.; Ohkuma, S. *J. Cell Biol.* **1981**, *90*, 665−669.

(23) Dautry-Varsat, A.; Ciechanover, A.; Lodish, H. F. *Proc. Natl. Acad. Sci. U. S. A.* **1983**, *80*, 2258−2262.

(24) Ang, A. L.; Taguch, T.; Francis, S.; Fölsch, H.; Murrells, L. J.; Marc Pypaert, G. W.; Mellman, I. *J. Cell Biol.* **2004**, *167*, 531−543.

(25) Gillooly, D. J.; Morrow, I. C.; Lindsay, M.; Gould, R.; Bryant, N. J.; Gaullier, J.-M.; Parton, R. G.; Stenmark, H. *EMBO J.* **2000**, *19*, 4577−4588.

(26) Uchida, Y.; Hasegawa, J.; Chinnapen, D.; Inoue, T.; Okazaki, S.; Kato, R.; Wakatsuki, S.; Misaki, R.; Koike, M.; Uchiyama, Y. *Proc. Natl. Acad. Sci. U. S. A.* **2011**, *108*, 15846−15851.

(27) Egami, Y.; Taguchi, T.; Maekawa, M.; Arai, H.; Araki, N. *Front. Physiol.* **2014**, *5*, 374.

(28) Ullrich, O.; Reinsch, S.; Urb, S.; Zerial, M.; Parton, R. G. *J. Cell Biol.* **1996**, *135*, 913−924.

(29) Weissleder, R.; Pittet, M. J. *Nature* **2008**, *452*, 580−589.




DOI: 10.1021/jacs.8b00277
J. Am. Chem. Soc. XXXX, XXX, XXX−XXX

(30) Frangioni, J. V. *Curr. Opin. Chem. Biol.* **2003**, *7*, 626−634.
(31) Lee, H.; Berezin, M. Y.; Guo, K.; Kao, J.; Achilefu, S. *Org. Lett.* **2009**, *11*, 29−32.
(32) Chai, X.; Cui, X.; Wang, B.; Yang, F.; Cai, Y.; Wu, Q.; Wang, T. *Chem. - Eur. J.* **2015**, *21*, 16754−16758.
(33) Fukazawa, A.; Suda, S.; Taki, M.; Yamaguchi, E.; Grzybowski, M.; Sato, Y.; Higashiyama, T.; Yamaguchi, S. *Chem. Commun.* **2016**, *52*, 1120−1123.
(34) Choi, H. S.; Nasr, K.; Alyabyev, S.; Feith, D.; Lee, J. H.; Kim, S. H.; Ashitate, Y.; Hyun, H.; Patonay, G.; Strekowski, L.; Henary, M.; Frangioni, J. V. *Angew. Chem., Int. Ed.* **2011**, *50*, 6258−6263.
(35) Kienast, Y.; von Baumgarten, L.; Fuhrmann, M.; Klinkert, W. E.; Goldbrunner, R.; Herms, J.; Winkler, F. *Nat. Med.* **2010**, *16*, 116−22.
(36) Lewis, J. D.; Destito, G.; Zijlstra, A.; Gonzalez, M. J.; Quigley, J. P.; Manchester, M.; Stuhlmann, H. *Nat. Med.* **2006**, *12*, 354−360.
(37) Liu, P.; Yue, C.; Sheng, Z.; Gao, G.; Li, M.; Yi, H.; Zheng, C.; Wang, B.; Cai, L. *Polym. Chem.* **2014**, *5*, 874−881.
(38) Maeda, H.; Wu, J.; Sawa, T.; Matsumura, Y.; Hori, K. *J. Controlled Release* **2000**, *65*, 271−284.
(39) Koeppen, B. M. *Adv. Physiol. Educ.* **2009**, *33*, 275−281.
(40) Hirakawa, Y.; Yoshihara, T.; Kamiya, M.; Mimura, I.; Fujikura, D.; Masuda, T.; Kikuchi, R.; Takahashi, I.; Urano, Y.; Tobita, S. *Sci. Rep.* **2016**, *5*, 17838.
(41) Raghunand, N.; Howison, C.; Sherry, A. D.; Zhang, S.; Gillies, R. J. *Magn. Reson. Med.* **2003**, *49*, 249−257.
(42) Helmlinger, G.; Sckell, A.; Dellian, M.; Forbes, N. S.; Jain, R. K. *Clin. Cancer Res.* **2002**, *8*, 1284−1291.
(43) Bourguignon, L. Y.; Singleton, P. A.; Diedrich, F.; Stern, R.; Gilad, E. *J. Biol. Chem.* **2004**, *279*, 26991−7007.
(44) Griffiths, J. R. *Br. J. Cancer* **1991**, *64*, 425−427.
(45) Gillies, R. J.; Liu, Z.; Bhujwalla, Z. *Am. Physiol. Soc.* **1994**, *267*, C195−C203.
(46) Robey, I. F.; Baggett, B. K.; Kirkpatrick, N. D.; Roe, D. J.; Dosescu, J.; Sloane, B. F.; Hashim, A. I.; Morse, D. L.; Raghunand, N.; Gatenby, R. A.; Gillies, R. J. *Cancer Res.* **2009**, *69*, 2260−2268.
(47) Gallagher, F. A.; Kettunen, M. I.; Day, S. E.; Hu, D. E.; Ardenkjaer-Larsen, J. H.; Zandt, R.; Jensen, P. R.; Karlsson, M.; Golman, K.; Lerche, M. H.; Brindle, K. M. *Nature* **2008**, *453*, 940−943.
(48) Saitoh, T.; Nakano, H.; Yamamoto, N.; Yamaoka, S. *FEBS Lett.* **2002**, *532*, 45−51.
(49) Nishimura, T.; Kaizuka, T.; Cadwell, K.; Sahani, M. H.; Saitoh, T.; Akira, S.; Virgin, H. W.; Mizushima, N. *EMBO Rep.* **2013**, *14*, 284−291.


DOI: 10.1021/jacs.8b00277
*J. Am. Chem. Soc.* XXXX, XXX, XXX−XXX